Inorg. Chem. **2003**, *42*, 3221–3228

Preparation and Magnetic Properties of $Mn(hfac)_2$-Complexes of 2-(5-Pyrimidinyl)- and 2-(3-Pyridyl)-Substituted Nitronyl Nitroxides

Keiji Okada,*,† Osami Nagao,† Hiroki Mori,† Masatoshi Kozaki,† Daisuke Shiomi,† Kazunobu Sato,† Takeji Takui,† Yasutaka Kitagawa,‡ and Kizashi Yamaguchi‡

Departments of Chemistry and Materials Science, Graduate School of Science, Osaka City University, Sugimoto, Sumiyoshi-ku, Osaka 558-8585, and Department of Chemistry, Graduate School of Science, Osaka University, Toyonaka, Osaka 560-0043, Japan

Received December 16, 2002

$Mn(hfac)_2$ complexes of [2-(5-pyrimidinyl)-4,4,5,5-tetramethyl-4,5-dihydro-1*H*- imidazoline-1-oxyl 3-oxide] (**1**) and its 2-(3-pyridyl) analogue (**2**) were prepared. Both complexes formed similar dimer structures. However, their packing patterns were considerably different. The pyrimidine dimers were aligned to form a linear chain structure, and each dimer was weakly bound by two sets of O6–C2 short contacts. In the pyridine dimer complex, two structurally similar but independent dimers were alternatively arranged, and two dimer–dimer contacts, O6–C2 (3.13 Å) and O6–C3 (3.30 Å), were observed. The pyrimidine complex showed strong antiferromagnetic behavior in the high temperature region (150–300 K) and weak ferromagnetic behavior below 100 K. Two models were used to analyze these magnetic properties. One is a quintet–septet thermal equilibrium model with mean-field approximation, which can reproduce the round minimum observed at about 150 K in $\chi_p T$ plots ($J_1/k_B = -148 \pm 2$ K with $\theta = +2.5 \pm 0.1$ K). The other is a ferromagnetic $S = 2$ chain model to fit the $\chi_p T$ values in the lower temperature region ($J_{S=2}/k_B = +0.31 \pm 0.01$ K). The pyridine complex showed antiferromagnetic interactions both in the high and low temperature regions. The magnetic behavior was similarly analyzed with the following parameters: $J_1/k_B = -140 \pm 2$ K with $\theta = -0.55 \pm 0.05$ K, and $J_{S=2}/k_B = -0.075 \pm 0.003$ K. The ligand–ligand interactions for both of the complexes were theoretically analyzed. The calculated results agreed well with the experiments. The stronger antiferromagnetic behavior observed in both the complexes at high temperatures was attributed to the magnetic interaction between the Mn(II) and the coordinating nitroxide oxygen atom. The weaker ferromagnetic interaction, $J_{S=2}/k_B = +0.31 \pm 0.01$ K, in the pyrimidine complex was attributed to the coulombic O6–C2 contact. Antiferromagnetic interaction $J_{S=2}/k_B = -0.075 \pm 0.003$ K in the pyridine complex was attributed to the O6–C3 contact.

Introduction

Recently, there has been a lot of interest in the magnetic properties of organic and inorganic materials and their composites. We have investigated the structure and magnetic properties of a composite system derived from organic radical-substituted ligands and magnetic metals.[1−3] In this system, metals can bind either ligands or radical centers, or both depending on the ligand structure and the metal, giving a variety of structures and their magnetic properties. In general, the magnetic interaction between metals and directly coordinating radicals is strong because of the short distance, although other factors such as orbital symmetry and the type of coordination are also important. The magnetic interaction through ligands (metal−ligand−radical) is weaker.[1,4]

We have previously shown that 5-pyrimidinyl-substituted nitronyl nitroxide, [2-(5-pyrimidinyl)-4,4,5,5-tetramethyl-4,5-dihydro-1*H*-imidazoline-1-oxyl 3-oxide] (**1**), affords a Cu-$(hfac)_2$ complex, $\mathbf{1}_2$·$[Cu(hfac)_2]_3$ (hfac = hexafluoroacetylacetonate).[5] The complex consists of a dimer defined by a

* To whom correspondence should be addressed. E-mail: okadak@sci.osaka-cu.ac.jp.
† Osaka City University.
‡ Osaka University.

(1) Kahn, K. In *Molecular Magnetism*; VCH Publishers: New York, 1993.
(2) (a) Caneschi, A.; Gatteschi, D.; Renard, J. P.; Rey, P.; Sessoli, R. *Inorg. Chem.* **1989**, *28*, 3314−3319. (b) Gatteschi, D.; Rey, P. In *Magnetic Properties of Organic Materials*; Lahti, P. M., Ed.; Marcel Dekker: New York, 1999; pp 601−625.
(3) Inoue, K.; Hayamizu, T.; Iwamura, H.; Hashizume, D.; Ohashi, Y. *J. Am. Chem. Soc.* **1996**, *118*, 1803−1804.
(4) Nagao, O.; Kozaki, M.; Shiomi, D.; Sato, K.; Takui, T.; Okada, K. *Polyhedron* **2001**, *20*, 1653−1658.

10.1021/ic0207193 CCC: $25.00
Published on Web 04/22/2003

Chart 1

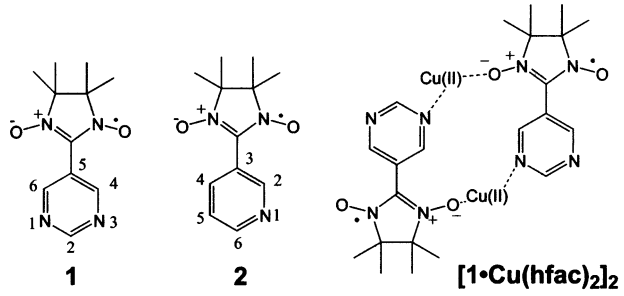

1 **2** **[1•Cu(hfac)$_2$]$_2$**

pair of **1**−Cu(hfac)$_2$ species, [**1**•Cu(hfac)$_2$]$_2$, and an almost magnetically free Cu(hfac)$_2$ in the crystalline state. The dimer structure was constructed with two pairs of coordination bonds, Cu(II)−O (nitronyl nitroxide) and Cu(II)−N (pyrimidine), as schematically shown in Chart 1. A strong antiferromagnetic interaction ($J/k_B = -1600$ K) between the nitronyl nitroxide and the Cu(II) was observed in the dimer structure. However, the magnetic interaction through the pyrimidine ring was too weak to observe. The dimer−dimer magnetic interaction was not observed because of the presence of magnetically isolated Cu(hfac)$_2$ between the dimers. Consequently, the overall magnetic property of this complex at low temperatures was governed by the magnetically free Cu(hfac)$_2$, leading to a paramagnetic behavior of the complex at temperatures as low as 1.9 K.

Because this dimer formation seems to be common in this type of ligand,[6] we wanted to explore dimer−dimer magnetic interactions using the dimer structure as a spin building block. To do this, dimers must be aligned at least in a one-dimensional way. Fortunately, Mn(hfac)$_2$ afforded the necessary structure with the composition of [**1**•Mn(hfac)$_2$]•0.5C$_6$H$_6$ (C$_6$H$_6$ as an incorporated solvent) where the dimers were aligned in a one-dimensional chain structure. In this paper, we report on the preparation and magnetic properties of [**1**•Mn(hfac)$_2$]•0.5C$_6$H$_6$ and a model complex, 2-(3-pyridinyl) nitronyl nitroxide [2-(3-pyridyl)-4,4,5,5-tetramethyl-4,5-dihydro-1*H*-imidazoline-1-oxyl 3-oxide] (**2**)−Mn(II) complex, [**2**•Mn(hfac)$_2$]$_2$, which has a similar dimer structure but a smaller positive charge on the C6-carbon (C2-carbon in the pyrimidine nomenclature) atom in the pyridiyl ligand than the one on the C2-carbon atom of [**1**•Mn(hfac)$_2$]•0.5C$_6$H$_6$.

Experimental Section

The chemicals were commercial grade, and they were used without further purification. Melting points were measured on a Yanako MP-J3 apparatus, and they are not corrected. Infrared spectra were measured on a Shimazu FT-IR-8700C. EPR spectra were recorded on a JEOL JFS-FE2XG. X-ray data were collected by a Rigaku RAXIS−RAPID imaging plate diffractometer using graphite monochromator Mo Kα radiation for both complexes. The structures were solved by a direct method (sir92), and they were expanded using a Fourier technique. All the calculations were performed using a teXsan crystallographic software package from the Molecular Structure Corporation. The magnetic susceptibility measurements were performed on a Quantum Design SQUID magnetometer, MPMS-XL. Compounds **1** and **2** were synthesized according to literature procedures.[7,8]

Preparation of [1•Mn(hfac)$_2$]•0.5C$_6$H$_6$. A suspension of 150.0 mg (0.32 mmol) of Mn(hfac)$_2$ in 30 cm^3 of *n*-heptane was refluxed for 1 h. Then the solvent (∼6 cm^3) was distilled as an azeotrope to remove water. This dried yellow Mn(hfac)$_2$ solution was added to a solution of 70.0 mg (0.29 mmol) of **1** in 5 cm^3 of dichloromethane. A dark-green powder immediately precipitated. Recrystallization of the powder from benzene−acetonitrile afforded 69 mg of black prisms in a 16% yield: C$_{21}$H$_{17}$F$_{12}$MnN$_4$O$_6$•0.5C$_6$H$_6$, fw 743.36, black prisms (benzene−acetonitrile), mp 163 °C. IR (KBr) 1651, 1496, 1338, 1257, 1195, 1141, 798, 709, 663, 582 cm^{-1}. Anal. Calcd for C$_{21}$H$_{17}$F$_{12}$MnN$_4$O$_6$•0.5C$_6$H$_6$: C, 38.78; H, 2.71; N, 7.54. Found: C, 38.67; H, 2.61; N, 7.54. EPR (powder) $g = 2.0081$ as a very broad monotonic signal with a width of 1027 G at half-height.

Preparation of [2•Mn(hfac)$_2$]$_2$. A heptane solution of dry Mn(hfac)$_2$ [prepared as described in the preceding paragraph, from 95 mg (0.20 mmol) of Mn(hfac)$_2$ in 20 cm^3 of *n*-heptane] was added to a solution of 45 mg (0.19 mmol) of **2** in 5 cm^3 of dichloromethane. The solution was left overnight at room temperature after which time a deep-blue powder precipitated. The precipitate was recrystallized from *n*-hexane to give 42 mg of deep-green prisms (30%): C$_{44}$H$_{34}$F$_{24}$Mn$_2$N$_6$O$_{12}$, fw 1406.64, deep-green prisms (*n*-hexane), mp 161 °C (decomp). IR (KBr) 1651, 1527, 1481, 1369, 1330, 1257, 1203, 1141, 798, 663, 582 cm^{-1}. Anal. Calcd for C$_{44}$H$_{34}$F$_{24}$Mn$_2$N$_6$O$_{12}$: C, 37.57; H, 2.58; N, 5.98. Found: C, 37.48; H, 2.46; N, 6.01. EPR (powder) $g = 2.0086$ as a very broad monotonic signal with a width of 750 G at half-height.

Calculation Method. The Gaussian 98 program[9] installed on an IBM RS6000 workstation was used in this study. In the UB3LYP calculations, 6-31G(d) basis sets were used. The geometries of the **1**−**1** and **2**−**2** pairs were taken from the X-ray structure of the complexes, [**1**•Mn(hfac)$_2$]•0.5C$_6$H$_6$ and [**2**•Mn(hfac)$_2$]$_2$. For the calculation of the low-spin broken-symmetry (BS) singlet states of these pairs, a trial UHF wave function for the SCF procedure was generated by the HOMO−LUMO mixing technique.[10] The criterion for the SCF convergence was 10^{-9}.

Results and Discussion

Structure of [1•Mn(hfac)$_2$]•0.5C$_6$H$_6$. Recrystallization of the crude dark-green powder of [**1**•Mn(hfac)$_2$] from an acetonitrile−benzene mixed solvent gave single crystals with a formula of [**1**•Mn(hfac)$_2$]•0.5C$_6$H$_6$ as a crystallographic

(5) Mori, H.; Nagao, O.; Kozaki, M.; Shiomi, D.; Sato, K.; Takui, T.; Okada, K. *Polyhedron* **2001**, *20*, 1663−1668.
(6) A similar dimer structure has also been reported: de Panthou, F. L.; Belorizky, E.; Calemezuk, R.; Luneau, D.; Marcenat, C.; Ressouche, E.; Turek, P.; Ray, P. *J. Am. Chem. Soc.* **1995**, *117*, 11247−11253.
(7) de Panthou, F. L.; Lunear, D.; Laugier, J.; Rey, P. *J. Am. Chem. Soc.* **1993**, *115*, 9095−9100.
(8) Davis, M. S.; Morokuma, K.; Kreilick, R. W. *J. Am. Chem. Soc.* **1972**, *94*, 5588−5592.
(9) Frisch, M. J.; Trucks, G. W.; Schlegel, H. B.; Scuseria, G. E.; Robb, M. A.; Cheeseman, J. R.; Zakrzewski, V. G.; Montgomery, J. A., Jr.; Stratmann, R. E.; Burant, J. C.; Dapprich, S.; Millam, J. M.; Daniels, A. D.; Kudin, K. N.; Strain, M. C.; Farkas, O.; Tomasi, J.; Barone, V.; Cossi, M.; Cammi, R.; Mennucci, B.; Pomelli, C.; Adamo, C.; Clifford, S.; Ochterski, J.; Petersson, G. A.; Ayala, P. Y.; Cui, Q.; Morokuma, K.; Malick, D. K.; Rabuck, A. D.; Raghavachari, K.; Foresman, J. B.; Cioslowski, J.; Ortiz, J. V.; Stefanov, B. B.; Liu, G.; Liashenko, A.; Piskorz, P.; Komaromi, I.; Gomperts, R.; Martin, R. L.; Fox, D. J.; Keith, T.; Al-Laham, M. A.; Peng, C. Y.; Nanayakkara, A.; Gonzalez, C.; Challacombe, M.; Gill, P. M. W.; Johnson, B. G.; Chen, W.; Wong, M. W.; Andres, J. L.; Head-Gordon, M.; Replogle, E. S.; Pople, J. A. *Gaussian 98*, revision A.11.3; Gaussian, Inc.: Pittsburgh, PA, 1998.
(10) Yamaguchi, K. *Chem. Phys. Lett.* **1975**, *33*, 330−335.

Table 1. Crystallographic Data for [**1**·Mn(hfac)$_2$]·0.5C$_6$H$_6$ and [**2**·Mn(hfac)$_2$]$_2$

	[**1**·Mn(hfac)$_2$]·0.5C$_6$H$_6$	[**2**·Mn(hfac)$_2$]$_2$
formula	$C_{21}H_{17}F_{12}MnN_4O_6\cdot0.5C_6H_6$	$C_{44}H_{36}F_{24}Mn_2N_6O_{12}$
fw	743.36	1406.64
cryst syst	triclinic	triclinic
space group	$P\bar{1}$ (No. 2)	$P\bar{1}$ (No. 2)
a/Å	10.259(1)	14.6353(6)
b/Å	16.377(1)	17.019(1)
c/Å	9.710(1)	14.420(2)
α/deg	94.382(2)	93.93(2)
β/deg	100.317(5)	117.656(9)
γ/deg	97.211(4)	110.81(1)
V/Å^3	1584.2(3)	2853.3(7)
Z	2	2
cryst size/mm^3	0.50 × 0.50 × 0.20	0.30 × 0.20 × 0.20
T/K	296	123
D_{calcd}/g cm^{-3}	1.558	1.637
F(000)	746.00	1408.00
μ/cm^{-1}	5.30 (Mo Kα)	5.82 (Mo Kα)
reflns measured	10515	16033
unique reflns	7170	12550
observation	5418 ($I > 3.0\sigma(I)$)	6873 ($I > 3.0\sigma(I)$)
R_1 [$I > 3\sigma(I)$][a]	0.049	0.061
R_w[b]	0.168	0.185
GOF	0.82	0.88
largest shift	0.177	0.035

[a] $R_1 = \sum||F_o| - |F_c||/\sum|F_o|$. [b] $R_w = [w(F_o^2 - F_c^2)^2/\sum w(F_o^2)^2]^{1/2}$.

repeating unit. The crystallographic data are summarized in Table 1. The two repeating units made a dimer with an inversion center (Figure 1a). The dihedral angle between the pyrimidine plane and the nitronyl nitroxide N−C−N plane in the ligand moiety was about 32°. The nitronyl nitroxide oxygen atom, O1, and the pyrimidine nitrogen atom, N1, were coordinated to the Mn(II) in a *cis*-configuration with the O1−Mn−N1 angle of 89.0° (Figure 1a). The lengths of the five Mn−O1−5 bonds were in the range 2.12−2.19 Å, and these bonds were a little shorter than the Mn−N1 bond (2.26 Å) (Table 2).

The dimers were aligned to form a linear chain along the *a* axis (Figure 1b). In the dimer−dimer contact, the two ligands were in a head-to-tail orientation. Each dimer was weakly bound by two equivalent short contacts between the nitroxide oxygen atom (O6) and pyrimidine carbon atom (C2) (O6−C2 contacts, 3.02 Å, Figure 1b). The contacts are shorter than the sum (3.29 Å) of the van der Waals radii of the oxygen atom (1.52 Å) and the aromatic sp^2-carbon (1.77 Å).[11] In this dimer orientation, the direction of the p-orbital of the O6 oxygen atom tilts by about 32° from the direction of the pπ-orbital of the C2 carbon of the pyrimidine ring. The angle is in the range of good orbital overlap to induce magnetic interactions.

Figure 1c shows a schematic diagram of possible magnetic interactions within and between the dimers; the direct coordination of O1 to Mn(II) should give the largest interaction, which is denoted by J_1, whereas the intradimer coordination of N1 to Mn(II) and the interdimer short contacts between C2 and O6 contribute to additional magnetic couplings, J_2 and J_3, which should be weaker than J_1. The sign and the magnitude of these interactions are discussed in the Magnetic Properties section.

(11) Bondi, A. *J. Phys. Chem.* **1964**, *68*, 441−451.

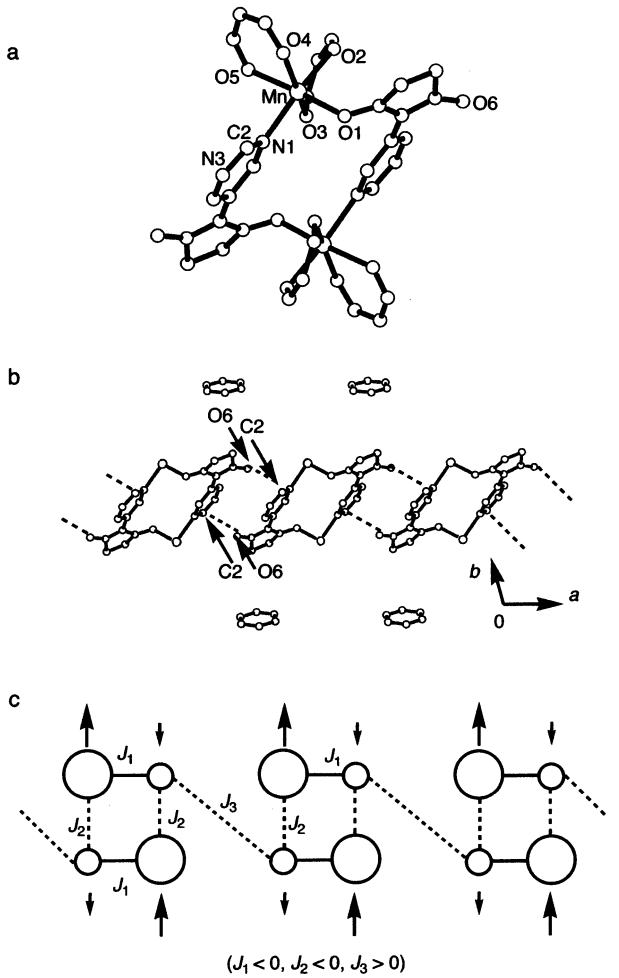

Figure 1. Crystal structure of [**1**·Mn(hfac)$_2$]·0.5C$_6$H$_6$. (a) Dimer structure. (b) One-dimensional structured chain of the dimers along the *a* axis. The hfac ligands are eliminated for clarity. The dashed lines indicate the interatomic short distances between the dimers. (c) Schematic diagram of the structured chain of $S_{Mn} = {}^5/_2$ and $S_R = {}^1/_2$ spins. The large and small circles denote the $S_{Mn} = {}^5/_2$ and $S_R = {}^1/_2$ spins, respectively. The solid lines represent the exchange interaction J_1 within the repeating unit. The dashed lines denote the exchange interactions J_2 and J_3 within and between the dimers, respectively. The arrows indicate the spin alignment in the ground state.

Table 2. Bond Lengths (Å) around Mn(II) for [**1**·Mn(hfac)$_2$]·0.5C$_6$H$_6$ and [**2**·Mn(hfac)$_2$]$_2$

	[**1**·Mn(hfac)$_2$]·0.5C$_6$H$_6$	[**2**·Mn(hfac)$_2$]$_2$
Mn−O1	2.131(2)	2.115(4),[a] 2.149(4)[b]
Mn−O2	2.188(2)	2.164(4),[a] 2.136(4)[b]
Mn−O3	2.170(2)	2.162(4),[a] 2.190(4)[b]
Mn−O4	2.119(2)	2.170(4),[a] 2.178(4)[b]
Mn−O5	2.180(2)	2.183(4),[a] 2.223(4)[b]
Mn−N1	2.262(2)	2.268(5),[a] 2.254(4)[b]

[a] For fragment **A** (Figure 2). [b] For fragment **B**.

Structure of [2·Mn(hfac)$_2$]$_2$. The crystallographic data for complex [**2**·Mn(hfac)$_2$]$_2$ are summarized in Table 1. Structurally similar but crystallographically independent dimers (**A** and **B**) with very different orientations as shown in Figure 2b were observed in a unit cell, which nearly doubled the cell volume as compared to that of [**1**·Mn(hfac)$_2$]·0.5C$_6$H$_6$. Each dimer had an inversion center, so that the overall structure was composed of two halves of dimers

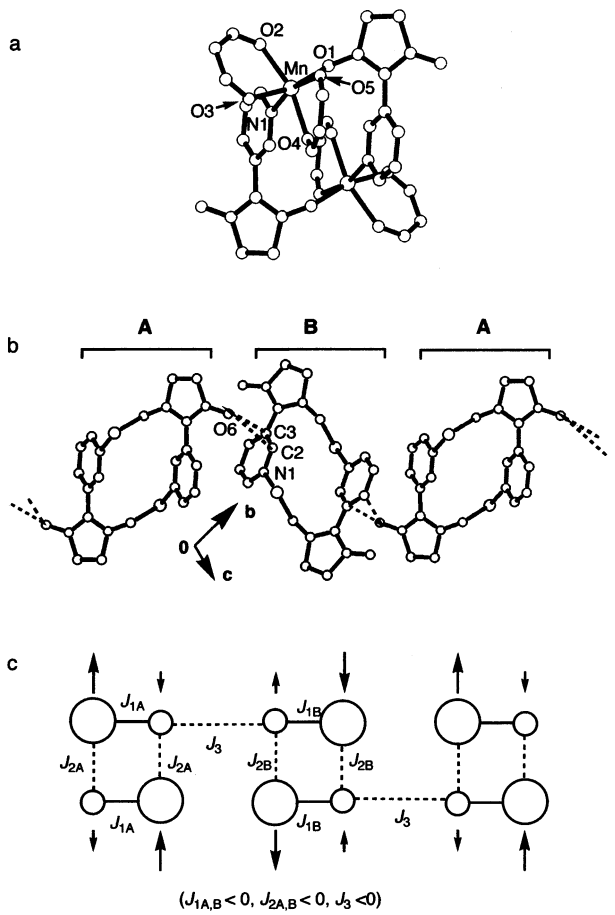

Figure 2. Crystal structure of [**2**·Mn(hfac)$_2$]$_2$. (a) Dimer structure. (b) One-dimensional structured dimer chain constructed by two independent dimers **A** and **B** along the [111] axis and the short contacts between the dimers. The hfac ligands are eliminated for clarity. (c) Schematic diagram of the structured chain of $S_{Mn} = {}^5/_2$ and $S_R = {}^1/_2$ spins. The large and small circles denote the $S_{Mn} = {}^5/_2$ and $S_R = {}^1/_2$ spins, respectively. The solid lines represent the exchange interaction J_1 within the repeating unit. The dashed lines denote the exchange interactions J_2 and J_3 within and between the dimers, respectively. The arrows indicate the spin alignment in the ground state.

A and **B** as a crystallographic repeating unit with formula [**2**·Mn(hfac)$_2$]$_2$.

The pyridine nitrogen and the nitroxide moiety were in a *cis*-configuration with the O1−Mn−N1 angles of about 85° (86.3° in **A** and 84.4° in **B**, Figure 2). The coordination bond lengths were in the range 2.12−2.22 Å for the Mn−O1−5 bonds and 2.25 and 2.27 Å for the Mn−N1 bond (Table 2). The dihedral angle between the nitronyl nitroxide plane and the pyridine ring was 43.7° for **A** and 38.7° for **B**. Although the overall dimer structures were very similar to that of the **1**-derived dimer, the pyridine dimer had a somewhat distorted geometry as determined from the bond angle (∼85°) of O1−Mn−N1 and the dihedral angle (∼41°) between the nitronyl nitroxide and pyridine planes.

A one-dimensional dimer chain extending in the [111] direction was found in [**2**·Mn(hfac)$_2$]$_2$ as depicted in Figure 2b, where the short contacts were observed in the adjacent two dimers, **A** and **B**: between the oxygen atom (O6) in dimer **A** and the C2- (3.13 Å) and C3-carbons (3.30 Å) of the neighboring dimer **B**. Although the O6−C2 contact was shorter than the O6−C3 contact, the p-orbital on the O6 atom was directed to the C3 carbon atom.

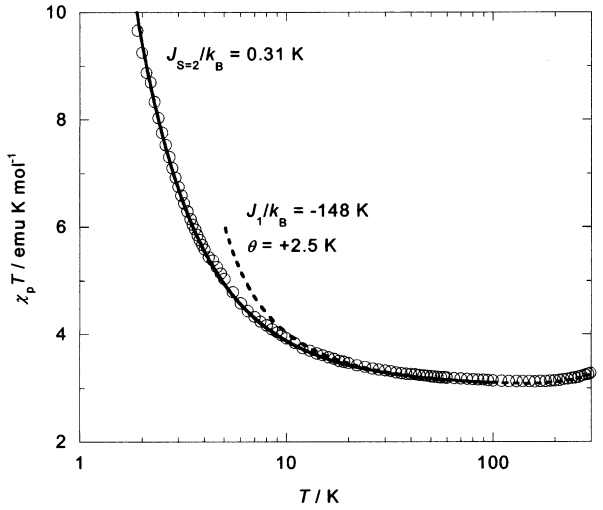

Figure 3. Magnetic susceptibility of [**1**·Mn(hfac)$_2$]·0.5C$_6$H$_6$ under a magnetic field of 1000 Oe in the χ_pT vs T plots. The solid line represents the simulation curve calculated from the ferromagnetic $S = 2$ chain model with $J_{S=2}/k_B = +0.31$ K, and the dashed line represents the spin-pair model with the mean-field approximation ($J_1/k_B = -148$ K, $\theta = +2.5$ K).

In the dimer−dimer contact, the two ligands were oriented in the head-to-head direction. As discussed in the Computational Analysis section, this head-to-head orientation may cause an antiferromagnetic interaction through the SOMO−SOMO orbital overlap.

The topology of the schematic diagram for the magnetic interactions is presented in Figure 2c, where interactions J_1 and J_2 for **A** and **B** are nonequivalent, and they are defined as $J_{1A} \neq J_{1B}$ and $J_{2A} \neq J_{2B}$ in a rigorous sense. For J_3, there are two alternative origins to be considered: the O6−(C2,-C3) contacts and the SOMO−SOMO overlap. In either case, the interaction can be treated as a nearest-neighbor nitroxide−nitroxide interaction in the Heisenberg approximation.

Magnetic Properties of [1·Mn(hfac)$_2$]·0.5C$_6$H$_6$. Figure 3 shows the temperature dependence of χ_pT for [**1**·Mn-(hfac)$_2$]·0.5C$_6$H$_6$. Crystallographic repeating unit [**1**·Mn-(hfac)$_2$]·0.5C$_6$H$_6$ was used as a magnetic repeating unit. The dimer structure involves two repeating units. The χ_pT value at 300 K was 3.28 emu K mol^{-1}, which is smaller than the sum (4.79 emu K mol^{-1}) of the χ_pT values expected for magnetically independent $S = {}^1/_2$ (0.378 emu K mol^{-1}) and $S = {}^5/_2$ (4.41 emu K mol^{-1}) spins assuming $g = 2.0081$. On lowering the temperature, the χ_pT value decreased to a round minimum of 3.13 emu K mol^{-1} at about 150 K, and it increased at lower temperatures as depicted in Figure 3.

The temperature dependence of the χ_pT values in the 150−300 K region indicates that the magnetic interactions are dominated by an antiferromagnetic coupling between the $S = {}^5/_2$ spin on the Mn(II) and the $S = {}^1/_2$ spin on the nitronyl nitroxide; thus, this strong antiferromagnetic interaction is assigned to J_1. The increase in χ_pT below 150 K indicates ferromagnetic interactions that are weaker than the antiferromagnetic interaction $|J_1|$. A plausible model for analyzing the temperature dependence of magnetic susceptibility for [**1**·Mn(hfac)$_2$]·0.5C$_6$H$_6$ is the structured chain depicted in

Figure 1c. Assuming that J_2 is negative and J_3 is positive (Figure 1c), the χ_pT value should increase at lower temperatures. When the spin−spin correlation as depicted in Figure 1c spreads over n repeating units, the χ_pT value reaches

$$\chi_pT = \frac{N_A g^2 \mu_B^2}{3k_B} \times 2n(2n+1)/n \quad (1)$$

with $S = 2n$. For instance, the χ_pT value observed at 1.9 K well exceeds 9.0 emu K mol^{-1}, which is the expected value for $n = 4$ repeating units with $S = 8$, i.e., two dimers, assuming $g = 2.0$. This clearly indicates that the spin−spin correlation as depicted in Figure 1c ($J_2 < 0$, $J_3 > 0$) develops over more than two dimers along the chain. Other combinations of signs for J_2 and J_3 cannot reproduce this high χ_pT value.

The magnetic coupling scheme in Figure 1c contains three coupling constants, J_1, J_2, and J_3 according to the crystal structure. It is, however, difficult to calculate magnetic susceptibility as a function of temperature with such a complicated coupling scheme. Here, the structured chain is approximated by the assemblage of a spin pair of $S_{Mn} = {}^5/_2$ on Mn(II) and $S_R = {}^1/_2$ on the radical with total spin $\mathbf{S}_{pair}$:

$$H_{pair} = -2J_1\mathbf{S}_{Mn}\cdot\mathbf{S}_R \quad (2)$$

$$\mathbf{S}_{pair} = \mathbf{S}_{Mn} + \mathbf{S}_R \quad (3)$$

The magnetic susceptibility is calculated by assuming a thermal equilibrium between the quintet ($S_{pair} = 2$) ground state and the excited septet ($S_{pair} = 3$) state of the repeating unit, the spin pair of $S_{Mn} = {}^5/_2$ and $S_R = {}^1/_2$:

$$E(S_{pair} = 2) = \frac{11}{4}J_1 \quad (4)$$

$$E(S_{pair} = 3) = -\frac{13}{4}J_1 \quad (5)$$

$$\chi_{pair} = \frac{N_A g_{av}^2 \mu_B^2}{3k_B(T-\theta)} \frac{30\exp[-E(S_{pair}=2)/k_BT] + 84\exp[-E(S_{pair}=3)/k_BT]}{5\exp[-E(S_{pair}=2)/k_BT] + 7\exp[-E(S_{pair}=3)/k_BT]} \quad (6)$$

The weaker exchange interactions, J_2 and J_3, are collectively approximated as a mean-field parameter θ in eq 6. The parameters J_1 and θ were optimized so as to reproduce the round minimum of χ_pT around 150 K, giving the estimates for the largest antiferromagnetic interaction and for additional interactions within the repeating units. Our best fitting was obtained with the interaction parameters of $J_1/k_B = -148 \pm 2$ K and $\theta = 2.5 \pm 0.1$ K with $g_{av} = 2.0081$ taken from the EPR spectrum (Figure 3).

The antiferromagnetic interaction of $J_1/k_B = -148$ K gives an energy gap of $\Delta E/k_B = 6J_1/k_B = -888$ K between the quintet ($S_{pair} = 2$) ground state and the excited septet ($S_{pair} = 3$) state within the repeating unit. Therefore, the structured chain is approximated by a linear chain of $S = 2$ below 100 K. Antiferromagnetic interaction J_2 between the $S_{Mn} = {}^5/_2$ and $S_R = {}^1/_2$ spins in the dimer gives rise to an apparently ferromagnetic interaction between the $S_{pair} = 2$ spins. Ferromagnetic interaction J_3 between the $S_R = {}^1/_2$ spins across the dimers affords a ferromagnetic interaction between the $S_{pair} = 2$ spins, giving a ferromagnetic zigzag chain of the $S_{pair} = 2$ spins. By neglecting the possible inequality for the two kinds of ferromagnetic interactions along the $S_{pair} = 2$ zigzag chain, a linear chain Hamiltonian of $S = 2$ spins with regular ferromagnetic interactions[12]

$$H_{S=2} = \sum_i [-2J_{S=2}\mathbf{S}^i\cdot\mathbf{S}^{i+1}] \quad (S = 2) \quad (7)$$

was fitted to the observed temperature dependence of χ_pT, where the $S = 2$ spins were treated as classical spins.[12] As shown by the solid curve in Figure 3, the ferromagnetic chain model of $S = 2$ reproduced the observed χ_pT with the ferromagnetic interaction of $J_{S=2}/k_B = +0.31 \pm 0.01$ K. Mean-field θ in eq 6 and ferromagnetic interaction $J_{S=2}$ in eq 7, both of which are collective approximate values for J_2 and J_3, indicate the ground state of the structured chain as a whole, as schematically shown by the arrows in Figure 1c.

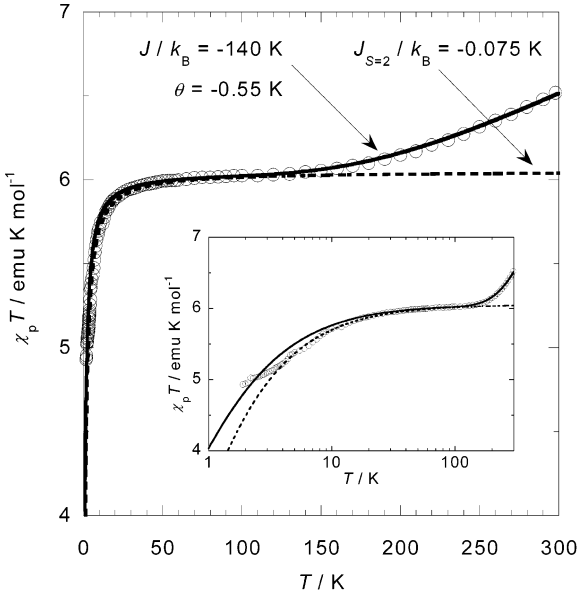

Figure 4. Magnetic susceptibility of [**2**·Mn(hfac)$_2$]$_2$ under a magnetic field of 1000 Oe in the χ_pT vs T plots. The solid line represents the simulation curve calculated from the spin-pair model with the mean field approximation ($J_1/k_B = -140$ K, $\theta = -0.55$ K), and the dashed line represents the simulation using the antiferromagnetic $S = 2$ chain model with $J_{S=2}/k_B = -0.075$ K. In the inset are depicted the χ_pT vs T plots in the logarithmic scale of temperature.

Magnetism of [2·Mn(hfac)$_2$]$_2$. Figure 4 shows the temperature dependence of χ_pT for [**2**·Mn(hfac)$_2$]$_2$. Crystallographic repeating unit [**2**·Mn(hfac)$_2$]$_2$ was used as a magnetic repeating unit to calculate the molar susceptibility, which contains half the moles of dimer **A** and half the moles of dimer **B**. The χ_pT value at room temperature was about 6.5 emu K mol^{-1}, which is smaller than the sum (9.59 emu K mol^{-1}) of the χ_pT values expected for 2 mol of magnetically independent $S = {}^1/_2$ spins (0.756 emu K mol^{-1}) of

(12) Fisher, M. E. *Am. J. Phys.* **1964**, *32*, 343−346.

nitronyl nitroxide and 2 mol of $S = {}^5/_2$ spins (8.83 emu K mol^{-1}) of Mn(II) assuming $g = 2.0086$. On lowering the temperature, the χ_pT value gradually decreased and approached a stationary value of 6.0 emu K mol^{-1}, which is close to the theoretical χ_pT value for 2 mol of $S = 2$. This temperature dependence of χ_pT suggests strong antiferromagnetic interactions between the Mn(II) and the directly coordinating nitronyl nitroxide oxygen atom, affording two $S = 2$ spins: one on a half of dimer **A** and the other on a half of dimer **B**. The χ_pT value dropped at lower temperatures, indicating a low-spin ground state of the chain of alternating aggregation of dimers **A** and **B**.

The magnetic interaction scheme of [**2**·Mn(hfac)$_2$]$_2$ is presented in Figure 2c. The $J_{1A,B}$ and $J_{2A,B}$ values are considered to be of the same sign and on the same order as J_1 and J_2, respectively, for the pyrimidine complex because of their structural similarity. This means that magnetic interaction J_3 should have a small negative value to account for the antiferromagnetic nature at low temperatures. The origin of J_3 may be in short contacts O6−C2 and O6−C3 or in the SOMO−SOMO orbital overlap caused by the head-to-head arrangement of the nitronyl nitroxides as previously described. The magnetic interaction scheme shown in Figure 2c is too complicated to be analyzed exactly. The two types of approximations were again used to determine the magnetic interactions in [**2**·Mn(hfac)$_2$]$_2$.

To estimate large antiferromagnetic interactions between the Mn(II) and the directly coordinating nitroxide, the thermal equilibrium model with a mean-field approximation, eqs 2−6, was used. The repeating unit for [**2**·Mn(hfac)$_2$]$_2$ is twice as large as that for the [**1**·Mn(hfac)$_2$]·0.5C$_6$H$_6$, and therefore, the numerator in eq 6 should be double for [**2**·Mn(hfac)$_2$]$_2$. Possible differences in the exchange interactions, $J_{1A} \neq J_{1B}$ and $J_{2A} \neq J_{2B}$, for dimers **A** and **B** were ignored to avoid overparametrization. Parameter J_1 in eqs 2 and 4−6 was regarded as an average one, $J_1 = (J_{1A} + J_{1B})/2$. Mean-field parameter θ in eq 6 approximates the other three exchange parameters, J_{2A}, J_{2B}, and J_3. The observed temperature dependence of χ_pT was reproduced with $J_1/k_B = -140 \pm 2$ K and $\theta = -0.55 \pm 0.05$ K with $g_{av} = 2.0086$ taken from the EPR spectrum (Figure 4). The determined J_1/k_B value is in good agreement with $J_1/k_B = -148 \pm 2$ K for [**1**·Mn(hfac)$_2$]·0.5C$_6$H$_6$.

The mean-field approximation in this model is too crude to reproduce the decrease in χ_pT in the low temperature region. The structured chain of [**2**·Mn(hfac)$_2$]$_2$ should be well approximated by an $S = 2$ zigzag chain at low temperatures. A regular chain model of $S = 2$ (eq 7) was adopted,[12] and all possible differences in the magnitude of the three $J_{S=2}$ values, corresponding to J_{2A}, J_3, and J_{2B}, along the zigzag chain were neglected. As depicted in Figure 4, the observed temperature dependence of χ_pT was reproduced by the $S = 2$ chain model with $J_{S=2}/k_B = -0.075 \pm 0.003$ K. Although the fitting of χ_pT is improved as compared to that in the described spin-pair model, the calculated χ_pT value deviates from the observed values below 3 K. The deviation may be attributed to the inequality of the $J_{S=2}$ values along the zigzag chain.

Computational Analysis of the Ligand−Ligand Contacts. The effective exchange integral (J_{ab}) between magnetic sites has been described by the Heisenberg (HB) model on experimental grounds as

$$H(\mathrm{HB}) = -2\sum J_{ab}\mathbf{S}_a\cdot\mathbf{S}_b \tag{8}$$

where $\mathbf{S}_a$ and $\mathbf{S}_b$ are spins at sites a and b, respectively. The recent development of computational techniques involving the calculation of open shelled species has enabled estimating J_{ab} values for various systems.[10,13−17] In particular, UHF methods have been found to be more effective than RHF-CI methods for larger molecular systems. We briefly describe the background for evaluating the exchange integral for open shelled systems with UHF methods. The problem occurs when one uses UHF methods to calculate low-spin states of open shelled polyradical systems with $S_{max} \geq 1$. Sometimes, magnetic orbitals for open shelled low-spin states are well approximated as localized orbitals only or mainly on one radical site or on parts in radical sites. Such states have different distributions of spins α and β. For UHF calculations, such a broken-symmetry (BS) wave function must first be generated. Furthermore, the low-spin state calculated using the SCF procedure exhibits spin-contamination contributed from the higher spin states. Therefore, establishing a suitable spin-projection procedure is also essential. Yamaguchi described the procedure of spin-projected UHF calculation in 1975.[10] Noodleman proposed a different method in 1981.[13,14] These procedures enable estimating J_{ab} values. There are currently three formulations that can be used to estimate J_{ab} values:

$$J_{ab}^{(1)} = \frac{{}^{\mathrm{LS}}E - {}^{\mathrm{HS}}E}{{S_{\max}}^2} \tag{9}$$

$$J_{ab}^{(2)} = \frac{{}^{\mathrm{LS}}E - {}^{\mathrm{HS}}E}{S_{\max}(S_{\max}+1)} \tag{10}$$

$$J_{ab}^{(3)} = \frac{{}^{\mathrm{LS}}E - {}^{\mathrm{HS}}E}{\langle {}^{\mathrm{HS}}S^2\rangle - \langle {}^{\mathrm{LS}}S^2\rangle} \tag{11}$$

where ${}^{\mathrm{LS}}E$, ${}^{\mathrm{HS}}E$, and S_{max} are, respectively, the total energies of the low-spin and high-spin states, and the maximum spin number of the system. The $J_{ab}^{(1)}$ derived by Noodleman is applicable to systems with a small overlap between magnetic orbitals.[13] The $J_{ab}^{(2)}$ derived by Ruiz is suitable for systems

(13) Noodleman, L. *J. Chem. Phys*. **1981**, *74*, 5737−5742.
(14) (a) Adao, C.; Barone, V.; Bencini, A.; Totti, F.; Ciofini, I. *Inorg. Chem.* **1999**, *38*, 1996−2004. (b) Eklund, J. C.; Bond, A. M.; Colton, R.; Humphrey, D. G.; Mahon, P. J.; Walter, J. W. *Inorg. Chem*. **1999**, *38*, 2005−2011.
(15) Ruiz, E.; Cano, J.; Alvarez, S.; Alemany, P. *J. Comput. Chem*., **1999**, 1391−1400.
(16) (a) Yamanaka, S.; Kawakami, T.; Nagao, H.; Yamaguchi, K. *Chem. Phys. Lett.* **1994**, *231*, 25−33. (b) Takano, Y.; Kitagawa, Y.; Onishi, T.; Yoshioka, Y.; Yamaguchi, K.; Koga, N.; Iwamura, H. *J. Am. Chem. Soc*. **2002**, *124*, 450−461 and references cited therein.
(17) (a) Yamaguchi, K.; Fukui, H.; Fueno, T. *Chem. Lett*. **1986**, 625−628. (b) Yamaguchi, K.; Fueno, T.; Nakasuji, K.; Murata, I. *Chem Lett*. **1986**, 629−632. (c) Yamaguchi, K. *Int. J. Quantum Chem*. **2002**, *90*, 370−385.

Table 3. Calculated Total Energies and Effective Exchange Integrals for the **1**−**1** Pair and **2**−**2** Pair in the Dimer−Dimer Contacts for [**1**·Mn(hfac)$_2$]·0.5C$_6$H$_6$ and [**2**·Mn(hfac)$_2$] Complexes

		BS-singlet state		triplet state		J (cm^{-1})		
pair	method/basis set	energy (au)	$\langle S^2\rangle$	energy (au)	$\langle S^2\rangle$	Yamaguchi	Noodleman	Ruitz
1−**1**	UB3LYP/6-31G*	−1594.53658688	1.1095	−1594.53662058	2.1099	+7.39	+7.40	+3.70
2−**2**	UB3LYP/6-31G*	−1562.31937556	1.1037	−1562.31935894	2.1040	−3.65	−3.65	−1.82

with a relatively large overlap.[15] Yamaguchi's $J_{ab}^{(3)}$ varies between the $J_{ab}^{(1)}$ and $J_{ab}^{(3)}$ values depending on the overlap.[16]

The dimer−dimer contacts are thought to be key to the bulk magnetization of these complexes, [**1**·Mn(hfac)$_2$]·0.5C$_6$H$_6$ and [**2**·Mn(hfac)$_2$]$_2$. Here, the geometries of the contacted ligand−ligand pairs, **1**−**1** and **2**−**2**, in the dimer−dimer contacts were extracted from the X-ray structure, and they were theoretically analyzed. Table 3 shows the total energies calculated using approximately spin-projected UB3LYP/6-31G(d),[16] and the effective exchange integral J_{ab} values calculated according to Yamaguchi's,[17] Noodleman's,[13] and Ruiz's[15] formulations. For the pyrimidine complex **1**−**1** pair, the total energy of the broken-symmetry (BS) singlet state is higher than that of the triplet state, and the exchange interaction is positive.[16] Since both **1**−**1** and **2**−**2** pairs are weak magnetic interaction systems, the agreement between the values of $J_{ab}^{(1)}$ and $J_{ab}^{(3)}$ is good. In contrast to the **1**−**1** pair of the pyrimidine complex, the **2**−**2** pair of the pyridine complex has a singlet ground state with a negative J_{ab} value. These results are qualitatively in good agreement with the experimental ones for both the complexes.

In the triplet and broken-symmetry singlet states, the **1**−**1** and **2**−**2** pairs have large SOMO coefficients on the nitrogen and oxygen atoms in the nitronyl nitroxide moieties. In the broken-symmetry singlet state, the SOMO orbitals are localized on one of the nitronyl nitroxide groups in both **1**−**1** and **2**−**2** pairs. In the **1**−**1** pair, the two nitronyl nitroxide groups are arranged in the head-to-tail direction, indicating that the SOMO−SOMO interaction is negligibly small. However, in the **2**−**2** pair, the two nitronyl nitroxides are in the head-to-head arrangement, indicating that the SOMO−SOMO orbital overlap may not be neglected.

The atomic spin densities and atomic charge for the **1**−**1** pair are listed in Table 4. The numbering of atoms is shown in Chart 2. The spin distribution pattern clearly indicates that the ferromagnetic interaction observed at low temperatures is brought about by the spin-polarization mechanism[14,16b,17a,b] through the O6−C2 contacts. Furthermore, it is also clear that the O6 oxygen atom (atom 2 or 15 in Table 4) has a large negative charge and the C2 carbon atom (atoms 20 or 7 in Table 4) has a large positive charge. These results indicate that the O2−C6 contacts observed in the X-ray analysis are based on the coulombic interaction.[18]

For the **2**−**2** pair, there are two factors to be considered: the short contacts (O6−C2 and O6−C3) and the SOMO−SOMO orbital overlap, as we already pointed out. In the SOMO−SOMO orbital interaction, the shortest oxygen−oxygen distance is 3.95 Å for atoms 2−15 (Chart 2). Although this distance is longer than the van der Waals sum (3.04 Å), it may still account for the small antiferromagnetic interaction. In order to estimate the contribution of the SOMO−SOMO overlap, we calculated the value of J_{ab} for a pyridyl-removed [2-hydro-4,4,5,5-tetramethyl-4,5-dihydro-1*H*-imidazoline-1-oxyl 3-oxide]$_2$ pair, where the atom coordinates except for the 2-hydrogens are exactly the same as in the **2**−**2** pair. This model pair afforded a positive $J_{ab}^{(1)} = +5.00$ cm^{-1} (UB3LYP/6-31G*). Therefore, the presence of pyridyl groups is essential to the negative J_{ab} value of the **2**−**2** pair. In the broken-symmetry singlet state of the **2**−**2** pair, the C3 (atom 21) carbon atom has a little larger spin density than the C2 (atom 22) carbon atom (Table 5).

Table 4. Calculated Atomic Spin Densities (Atomic Charges) for the Selected Atoms in the Contacting **1**−**1** Pair of [**1**·Mn(hfac)$_2$]·0.5C$_6$H$_6$ Complex

	atom (code in text)	triplet state spin density (charge)	broken symmetry state spin density (charge)
1	O	+0.343 (−0.469)	+0.343 (−0.469)
2	O (O6)	+0.344 (−0.472)	+0.344 (−0.472)3
3	N	+0.271 (−0.121)	+0.271 (−0.121)
4	N	+0.269 (−0.078)	+0.269 (−0.078)
5	N	+0.014 (−0.417)	+0.012 (−0.417)
6	N	+0.015 (−0.427)	+0.012 (−0.427)
7	C (C2)	−0.028 (+0.380)	−0.027 (+0.380)
8	C	−0.031 (+0.265)	−0.029 (+0.265)
9	C	+0.041 (+0.068)	+0.039 (+0.068)
10	C	−0.035 (+0.245)	−0.033 (+0.245)
11	C	−0.219 (+0.489)	−0.218 (+0.489)
12	C	−0.016 (+0.126)	−0.016 (+0.126)
13	C	−0.015 (+0.063)	−0.015 (+0.063)
14	O	+0.343 (−0.469)	−0.343 (−0.469)
15	O (O6)	+0.344 (−0.472)	−0.344 (−0.472)
16	N	+0.271 (−0.121)	−0.271 (−0.121)
17	N	+0.269 (−0.077)	−0.269 (−0.077)
18	N	+0.014 (−0.416)	−0.012 (−0.416)
19	N	+0.015 (−0.426)	−0.012 (−0.426)
20	C (C2)	−0.028 (+0.380)	+0.027 (+0.380)
21	C	−0.030 (+0.265)	+0.029 (+0.265)
22	C	+0.041 (+0.067)	−0.039 (+0.067)
23	C	−0.035 (+0.245)	+0.033 (+0.245)
24	C	−0.219 (+0.489)	+0.218 (+0.489)
25	C	−0.016 (+0.126)	+0.016 (+0.126)
26	C	−0.015 (+0.062)	+0.015 (+0.062)

Chart 2

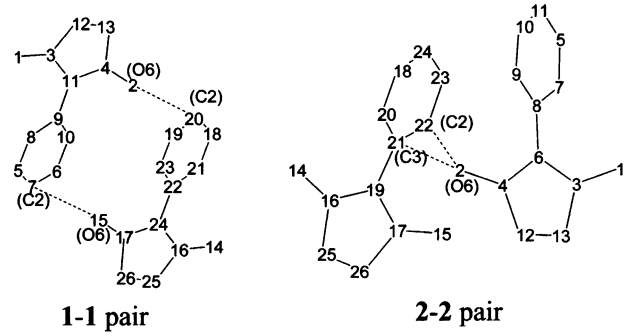

(18) Magnetic interaction through coulombic interaction is precedented: Awaga, K.; Yamaguchi, A.; Okuno, T.; Inabe, T.; Nakamura, T.; Matsumoto, Y.; Maruyama, Y. *J. Mater. Chem.* **1994**, *4*, 1377−1385.

Table 5. Calculated Atomic Spin Densities (Atomic Charges) for the Selected Atoms in the Contacting **2**−**2** Pair of [**2**·Mn(hfac)$_2$] Complex

	atom (code in text)	triplet state spin density (charge)	broken symmetry state spin density (charge)
1	O	+0.345 (−0.473)	+0.345 (−0.473)
2	O (O6)	+0.346 (−0.486)	+0.346 (−0.486)
3	N	+0.259 (−0.095)	+0.259 (−0.095)
4	N	+0.268 (−0.080)	+0.268 (−0.080)
5	N	+0.010 (−0.447)	+0.010 (−0.447)
6	C	−0.215 (+0.481)	−0.215 (+0.481)
7	C	−0.024 (+0.238)	−0.024 (+0.238)
8	C	+0.035 (+0.089)	+0.035 (+0.089)
9	C	−0.025 (+0.075)	−0.025 (+0.075)
10	C	+0.012 (−0.006)	+0.012 (−0.006)
11	C	−0.023 (+0.206)	−0.023 (+0.206)
12	C	−0.015 (+0.073)	−0.015 (+0.073)
13	C	−0.014 (+0.067)	−0.014 (+0.067)
14	O	+0.368 (−0.464)	−0.368 (−0.464)
15	O	+0.321 (−0.493)	−0.321 (−0.493)
16	N	+0.265 (−0.105)	−0.266 (−0.105)
17	N	+0.273 (−0.093)	−0.273 (−0.093)
18	N	+0.012 (−0.450)	−0.012 (−0.450)
19	C	−0.219 (+0.488)	+0.219 (+0.488)
20	C	−0.029 (+0.263)	+0.029 (+0.263)
21	C (C3)	+0.040 (+0.103)	−0.039 (+0.103)
22	C (C2)	−0.032 (+0.039)	+0.032 (+0.039)
23	C	+0.017 (−0.007)	−0.016 (−0.007)
24	C	−0.027 (+0.217)	+0.028 (+0.217)
25	C	−0.016 (+0.053)	+0.016 (+0.053)
26	C	−0.014 (+0.111)	+0.014 (+0.111)

The spin-polarization mechanism through the O6−C3 contact can well explain the low-spin ground state of the **2**−**2** pair. The importance of this longer contact can be ascribed to the C3-directed orientation of the magnetic orbital on the O6 atom as described in the structure section.

Conclusion

The structures and magnetic properties of two complexes, [**1**·Mn(hfac)$_2$]·0.5C$_6$H$_6$ and [**2**·Mn(hfac)$_2$]$_2$, were studied. Both complexes formed similar dimer structures with considerably different packing patterns. The **1**-derived dimers were aligned in a one-dimensional way along the *a*-axis. A dimer−dimer contact was observed between the O6 atom and the C2 atom in the nearest dimer. In the **2**-derived dimers, two structurally similar but independent dimers were observed in a unit cell. They were alternately aligned as a one-dimensional chain along the [111] axis. A dimer−dimer contact was observed between the O6 atom and the C2 and C3 carbons in the nearest dimer. In accordance with these differences in the packing structure, their magnetic properties were also very different. Complex [**1**·Mn(hfac)$_2$]·0.5C$_6$H$_6$ showed a strong antiferromagnetic interaction in the high temeperature region (300−150 K) and a weak ferromagnetic interaction at temperatures below 100 K. Two models were used to analyze the temperature dependence of $\chi_p T$. A quintet−septet thermal equilibrium model with mean-field approximation enabled estimating a strong antiferromagnetic interaction with a weaker mean-field ferromagnetic parameter: $J_1/k_B = -148 \pm 2$ K with $\theta = +2.5 \pm 0.1$ K. The ferromagnetic interaction observed at low temperatures was analyzed using a ferromagnetic $S = 2$ chain model with $J_{S=2}/k_B = +0.31 \pm 0.01$ K. Complex [**2**·Mn(hfac)$_2$]$_2$ showed strong and weak antiferromagnetic interactions. These antiferromagnetic interactions were estimated by using similar methods, i.e., mean-field approximation with $J_1/k_B = -148 \pm 2$ K and $\theta = -0.55 \pm 0.05$ K and an antiferromagnetic $S = 2$ chain model with $J_{S=2}/k_B = -0.075 \pm 0.003$ K.

The strong antiferromagnetic behavior in both the complexes is obviously based on the interaction between Mn(II) and the coordinating nitroxide oxygen atom. In order to assign the weaker interaction, the ligand−ligand contacts in these dimer−dimer contacts were theoretically studied, and their exchange interactions, spin densities, and atomic charges were calculated. The calculated results were in good agreement with the experimental ones.

The weaker ferromagnetic interaction, $J_{S=2}/k_B = +0.31 \pm 0.01$ K, in the pyrimidine complex was assigned to the coulombic O6−C2 short contact structure, through which a ferromagnetic coupling would arise via the spin-polarization mechanism. The assignment of the antiferromagnetic interaction, $J_{S=2}/k_B = -0.075 \pm 0.003$ K, in the pyridine complex was a little complicated because of the two alternative factors to be considered, the SOMO−SOMO orbital interaction and the short ligand−ligand contacts (O6−C3 and O6−C2). The calculation for a pyridyl-removed model compound showed that the presence of pyridyl rings was essential to the antiferromagnetic interaction of the **2**−**2** pair. Thus, the weak antiferromagnetic interaction of $J_{S=2}/k_B = -0.075 \pm 0.003$ K was attributed to the short dimer−dimer contacts (O6−C3 and O6−C2). The observed antiferromagnetic interaction can be explained assuming that the spin-polarization mechanism via the O6−C3 contact is predominant. Further studies of the structure−magnetism relationships of related organic and inorganic composite systems are in progress.

Acknowledgment. We would like to thank the Ministry of Education, Science, Sports, and Culture of Japan for a Grant for Scientific Research in a Special Field, No. 10146101).

Supporting Information Available: Tables of X-ray crystallographic data in CIF formats for [**1**·Mn(hfac)$_2$]$_2$·C$_6$H$_6$ and [**2**·Mn(hfac)$_2$]$_2$ and tables of the spin densities and atomic charges for all the atoms of **1**−**1** and **2**−**2** pairs. This material is available free of charge via the Internet at http://pubs.acs.org.

IC0207193